RESEARCH ARTICLE

Alternative methods for the pilot-scale production and characterization of chitosan nanoparticles

Helton José Alves[1] · Lázaro José Gasparrini[1] · Felipe Eduardo Bueno Silva[1] · Laressa Caciano[1] · Graciela Ines Bolzon de Muniz[2] · Eduardo Luis Cupertino Ballester[3] · Paulo André Cremonez[1] · Mabel Karina Arantes[1]

Abstract

This work describes the production/characterization of low molar mass chitosan nanoparticles derived from waste shrimp shells (SSC), as well as from a commercial chitosan (CC). The production of low molar mass nanochitosan employed thermal shock, alternating between 100 °C and ambient temperature, followed by grinding the dry material (SSC and CC) in a ball mill, producing around 500 g of nanochitosan per batch. A highlight of the methodology employed is that it enables nanochitosan to be obtained even from a low quality commercial raw material. All particles had diameters smaller than 223 nm, with an average diameter below 25 nm (determined by DLS), while reductions of molar mass were between 8.4-fold and 13.5-fold. The depolymerization process resulted in a reduction in crystallinity of 38.1 to 25.4% and 55.6 to 25.9% in the CC and SSC samples, respectively. The production of nanochitosans was also confirmed by TEM through the observation of crystalline domains with diameters between 5 and 10 nm. This work perfectly reproduces the results on bench scale from previous research. The simple and inexpensive processes enable easy scale-up, representing an important advance in the production chain of biopolymers.

Keywords Nanopolymers · Depolymerization · Nanomaterials · Scale-up, Biopolymer · Waste management

Introduction

Chitosan nanoparticles have been studied, produced, and employed in different areas, taking advantage of the useful characteristics of this biopolymer. Chitosan has been extensively characterized and is used in biomedicine, drug delivery, gene therapy, tissue engineering, and as biomarker for bioimaging (Egladir et al. 2015; Muanprasat and Chatsudthipong 2017; Mitall et al. 2018). It is used in food to reduce cholesterol (Panit et al. 2016; van der Gronde et al. 2016), as well as for environmental (Wang et al. 2009; Gupta et al. 2017) and agricultural (Wu and Liu 2008; Perez et al. 2018) applications, among others. This is due to its favorable features such as biodegradability, biocompatibility, nontoxicity, microbial activity, and capacity for cross-linking and hydrogel formation (Perez and Francois 2016; Bakshi et al. 2018).

The properties of chitosan, such as its hydrophobicity, solubility, and viscosity, are influenced by variations of its main characteristics, especially the degree of deacetylation (usually between 70 and 95%) and the molar mass (which varies from 10 to 10^3 kDa) (Arantes et al. 2014). The polymer obtained in the form of nanoparticles is of particular interest, due to aspects such as increased specific area of the particles, the availability of reactive groups, the surface energy, homogeneous particle size, and other morphological features (Nagpal et al. 2013; Mitall et al. 2018), in addition to high solubility and low viscosity of the solutions.

Many studies have investigated the production of chitosan nanoparticles, involving the development of new

✉ Paulo André Cremonez
pa.cremonez@gmail.com

1 Laboratory of Materials and Renewable Energy (LABMATER), Department of Engineering and Exact, Federal University of Paraná – UFPR, Rua Pioneiro 2153, Jardim Dallas, Palotina, PR 85950-000, Brazil

2 Department of Forest Engineering and Technology, Federal University of Paraná, Av. Pref. Lothario Meissner, 900, Jardim Botânico, Curitiba, PR 80210-170, Brazil

3 Laboratory of Shrimp (LABCAR), Department of Zootechnics, Federal University of Paraná – UFPR, Rua Pioneiro 2153, Jardim Dallas, Palotina, PR 85950-000, Brazil

methodologies and the improvement of existing techniques. Various methods can be used to form chitosan nanoparticles, such as electrospray, emulsification, solvent diffusion, and micro-emulsion procedures. Of particular interest is the ionic gelation technique, which employs an anionic cross-linking agent, usually tripolyphosphate (TPP), where the NH_3^+ groups of the acidified chitosan form cross-links with the TPP anions, leading to three-dimensional arrangements that compose chitosan nanoparticles (Carvalho et al. 2019; Ye et al. 2018; Pant and Negi 2018; Soares et al. 2016).

The ionic gelation method is relatively simple, compared with many other techniques. However, it has some limitations, such as the influence of the molar mass of the chitosan, since longer chains hinder the interaction between chitosan and the TPP groups, leading to formation of large particles, which has also been observed for degrees of deacetylation exceeding 85% (Tang et al. 2007). Another frequently reported problem is related to dispersivity of chitosan-TPP nanoparticles, associated with the occurrence of larger particles, which provide effective encapsulation (of drugs, for example), but present low delivery efficiency. Fan et al. (2012) reported that it was necessary to use low molar mass chitosan and high ionic strength TPP solution to overcome this problem. In order to avoid the formation of large particles and their aggregation, an additional process step can be employed, with formation of an intermediate complex between the TPP and a cross-linking agent, so that only nanoparticles are formed Pant and Negi 2018). Rigid and resistant nanoparticles can be obtained by ionic gelation, although this requires a high TPP/chitosan mass ratio in the range from 0.09 to 0.18 (Carvalho et al. 2019).

Considering these issues, the methodology presented here for obtaining chitosan nanoparticles offers some important advantages, since the process enables a high degree of depolymerization of chitosan, with a substantial reduction of molar mass, together with formation of particles with nanometric dimensions (nanoparticles). Purely physical methods (drying and grinding), which already comprise part of the chitosan production route, are used to achieve these two goals. In work reported in the literature, these effects are obtained using separate processes: (i) production of chitosan, (ii) depolymerization, and (iii) production of chitosan nanoparticles. Furthermore, the depolymerization requires sophisticated techniques and/or inputs that can hinder scale-up, in addition to leading to prohibitive costs (Alves et al. 2018).

Despite promising results, studies describing the characteristics of the nanopolymers obtained are extremely scarce, especially concerning nanochitosan derived from different sources of raw material. Therefore, the aim of the present work was to characterize chitosan nanoparticles produced at a pilot scale (500 g per batch) from two sources: chitin from freshwater shrimp shells and commercial chitosan. Evaluation was made of the efficiency of a sequence of physical processes for the production of low molar mass chitosan nanoparticles,

followed by characterization of the most important properties of the nanopolymer using a range of robust analytical techniques.

Methodology

Origins and characteristics of the chitosans

Commercial chitosan

The commercial chitosan used in this work was manufactured and marketed by a Brazilian company and had a minimum 85% degree of deacetylation and ash content ≤ 1.5% (data provided by the supplier). No molar mass information was provided. The chitosan presented a yellowish color, with a lack of homogeneity among batches, and was difficult to fully solubilize in acetic acid (1.0% w/v). Due to the likelihood of impurities present in the material and the lack of information about the molar mass, characterizations were performed using SEM/EDS and viscometry (as described in "Characterization of the chitosan samples before and after the physical treatments"), respectively, in order to elucidate these aspects.

Chitosan obtained from freshwater shrimp shells

The cephalothoraxes of the shrimps were cleaned, washed, and dried, followed by grinding in a hammer mill and sieving until the particles passed easily through a mesh with 63-μm openings. Batches of 500 g of material were prepared, and the ground shells were washed twice with 0.55 mol L^{-1} HCl, for demineralization. The material was then washed twice with 0.3 M NaOH, at 80 °C, for deproteinization. Next, deacetylation was performed by refluxing the material at 110 °C for 10 h in 60% (w/v) NaOH solution, using a chitin proportion of 2.5% (w/v). The methodology adopted for production of the shrimp shell chitosan was adapted from the procedure described by Alves et al. (2018).

Production of nanochitosan

The methodology adopted for production of nanochitosan was based on thermal shock followed by grinding of the dry material, as described previously by Alves et al. (2018), with some modifications. The experiments were designed to enable the pilot-scale production of about 500 g of chitosan nanoparticles per batch, using appropriately sized tanks and equipment.

Pretreatment of the chitosan prior to application of thermal shock

The shrimp shell (SSC) was solubilized at a proportion of 2% (w/v) in 15% (w/v) acetic acid solution, under mechanical

stirring for 17 h, at ambient temperature. It was then precipitated using 2 M NaOH in a proportion of 1:1 (v/v), obtaining a chitosan gel that was washed with distilled water until reaching pH 7, followed by filtering.

The commercial chitosan (CC) received a similar pretreatment, with the exception of the solubilization step. This material was solubilized in HCl at a concentration of 0.55 mol L^{-1}, due to the possible presence of minerals that could limit its solubility in 1% (w/v) acetic acid.

Thermal shock treatment

After the precipitation step, the material was spread in a thin layer on a non-stick surface and subjected to thermal shock (alternating between 100 °C and ambient temperature) for 3 h, using cycles of 10 min in an oven and 5 min at room temperature outside the oven.

Milling

After drying, the material was ground in a ball mill (Model SL-34, Solab) consisting of an AISI 1020 steel vessel (14 cm diameter and 20 cm height) and an induction motor operated at a fixed speed of 300 rpm. Ceramic balls (20 mm spheres) were used in a proportion of 4 kg of balls to 86 g of chitosan. The milling was continued for 4.5 h to obtain particles smaller than 1 mm, which were then passed through a sieve with mesh openings of 106 μm (Alves et al. 2018). The material that did not pass through the sieve during the stipulated time was resubmitted to the grinding process until the required particle size was reached.

Characterization of the chitosan samples before and after the physical treatments

Physicochemical characterization

The ash contents of the samples, representing the inorganic material present, were determined by first drying the materials at 110 °C until constant mass, followed by incineration at 800 °C in an electric muffle furnace for sufficient time to obtain a constant mass of ash. The ash content was then calculated as the ratio between the final mass of the incinerated sample and the initial dry mass.

For determination of the protein content, the chitosan samples were treated by the alkaline deproteinization technique (using 0.3 M NaOH at 80 °C), with measurement of the protein content in the supernatant using an adaptation of the standard Biuret protein assay (Neves et al. 2017; Rao and Stevens 2006).

The mean viscometric molar mass of the chitosan samples was determined from the intrinsic viscosity of diluted chitosan solutions, using the relationship between the intrinsic viscosity and the mean viscometric molar mass of the polymer, according to the Mark-Houwink-Sakurada equation (Kasaai 2007). An Ubbelohde dilution viscometer with a 0.44-mm capillary (Cannon Instrument Co., USA) was used to obtain the intrinsic viscosity of solutions of chitosan at concentrations between 0.31 and 0.73 mg mL^{-1} in 0.3 M HAc/0.2 M NaOAc (Alves et al. 2018).

The degree of deacetylation (DD) of the chitosan samples was determined by conductometric titration of acid solutions of chitosan with NaOH solution, as described by Santos et al. (2009).

Hydrodynamic diameter determination by dynamic light scattering

For the DLS analyses, the chitosan samples were diluted in 2% (v/v) acetic acid solution, agitated for 48 h at 125 rpm and ultrasonicated for 15 min to improve dispersion of the particles.

The hydrodynamic size distribution of the particles was determined using a Bettersize Nanoptic 90 instrument, at a wavelength of 635 nm, dispersion angle of 90°, and temperature of 31 °C.

X-ray diffraction

XRD analyses were performed using a Bruker D2 PHASER diffractometer operated using Cu Kα radiation (1.5418 Å), at 30 kV, 10 mA, with continuous scanning at 0.01°, time scale of 1 s, and readings acquired in the 2θ range 5–60°. DIFFRAC.EVA software was used to interpret the results and evaluate the crystallinity of the material.

Scanning electron microscopy

SEM analyses were performed using a Quanta 440 microscope FEI coupled to an energy-dispersive spectroscopy (EDS) system to enable semiquantitative determination of the chemical compositions of the samples. Prior to analysis, the powdered materials were dispersed onto double-sided carbon tape, followed by sputter-coating with a fine layer of gold.

Transmission electron microscopy

Transmission electron microscopy analyses of the nanochitosan samples were performed with a TECNAI G^2 F20 instrument FEI operated at 200 kV, with a STEM spot size of 8. The powdered sample was previously dispersed in isopropyl alcohol, under ultrasonication for 30 min, followed by transfer of an aliquot to a copper grid coated with a thin carbon film and drying at ambient temperature. Analyses in high-resolution mode (HRTEM) were performed under cryogenic conditions, at liquid N$_2$ temperature (− 178 °C), because

in the absence of cooling, heating by the electron beam could cause decomposition of the biopolymer.

Results and discussion

Table 1 shows the results obtained for the ash content, protein concentration, degree of deacetylation (DD), and viscometric molar mass (MMv) of the chitosans. The properties of the two chitosans were quite similar, both before and after the thermal shock depolymerization step. The DD values could not be considered high, since they did not exceed 75% (Tsai et al. 2002; Arantes et al. 2014), but their similarity was of interest from the perspective of comparing the properties of the two materials. Since the depolymerization method used in this work involved only physical processes, the DD values remained unchanged. It should be noted that the DD value of 73% for the CC sample before depolymerization was lower than the value of 85% indicated by the manufacturer. For a sample to be considered as chitosan, the DD should exceed 50% (Gonil and Sajomsang 2012), making it soluble in an acid medium (Rinaudo 2006).

The protein concentrations obtained for the chitosans were extremely low and below the detection limits of the analytical method used. A low protein concentration is a desirable feature for a good quality chitosan.

The processing treatment applied to the chitosans resulted in MMv reductions of 13.5-fold for the SSC (from 243 to 18 kDa) and 8.4-fold for the CC (from 177 to 21 kDa). The final MMv values were approximately 7% and 12% of the original values for the SSC and CC, respectively.

The ash content of the CC chitosan increased considerably after the depolymerization process, from 1.38 to 2.57%, which could be explained by the use of hydrochloric acid (HCl) during the thermal shock step. The supply of chloride ions enabled the formation of NaCl, since the subsequent precipitation step involved pouring the solution into a tank containing sodium hydroxide (NaOH), in order to precipitate the nanochitosan, so the NaCl consequently contributed to the ash content.

High percentages of ash usually result in a higher concentration of particulate matter when the material is solubilized in weak acidic solutions. The incomplete solubilization of the material limits its use in certain applications that require greater purity of the material, as is the case in the pharmaceutical and medical sectors. Therefore, the method used for depolymerization of the CC was highly efficient from the point of view of reducing the molar mass of the biopolymer but could have compromised the quality of the material in terms of its solubility.

The EDS analysis revealed the presence of substantial amounts of Fe, Ca, Si, and Na in the ash of the CC chitosan prior to the depolymerization process (Table 2), while the ash of CCD (the commercial chitosan after depolymerization) had an even higher Na content, in addition to the presence of Cl. This provided further evidence that the increase in the ash content of the samples was associated with the formation of NaCl during the stage of precipitation of the CC, among other factors. The presence of Fe and Cr indicated the existence of impurities in the CC sample, with these metals in solution being able to interact with the biopolymer, forming complex ions (Wang et al. 2005; Zimmermann et al. 2010) and affecting the color of the product, as well as other properties such as viscosity.

Dynamic light scattering

DLS analysis was used to obtain the relative number distributions of particles of different diameters present in the sample solution (Alves et al. 2018). Substantial differences were observed in the particle diameter distribution profiles before/after depolymerization (Fig. 1). The results obtained to particle volume (Fig. 1a) showed that the chitosan samples before depolymerization (CC and SSC) had higher concentration of particle diameters between 900 and 1300 nm. In the case of the low molar mass CCD and SSCD samples, which had been subjected to thermal shock, all of the particles presented diameters below 223 nm. There were high concentrations of particles in the size range between 60 and 90 nm, as well as particles with smaller diameters of up to 15 nm, so these materials could be considered as nanochitosans. Similar trends were observed for the DLS results presented in terms of the particle number distributions (Fig. 1b), with samples CC and SSC showing particle size distributions covering a larger diameter range, while the diameters of the CCD and SSCD chitosans presented maxima of 160 nm after depolymerization. The mean particle diameter (D_{50}) of the SSCD nanochitosan was smaller than that of CCD material, with values of 62.1 and 87 nm, respectively.

The results confirmed that the methodologies employed for processing of the SSC chitosan and depolymerization of the CC were suitable strategies for obtaining nanochitosan. The reduction of the molar mass of the biopolymer by thermal

Table 1 Characterization of the chitosans before and after depolymerization

Test	SSC		CC	
	Before dep.	After dep.	Before dep.	After dep.
Ashes (%)	1.43	1.54	1.38	2.57
Protein (mg mL^{-1})	0.025	-	0.040	-
DD (%)	75	-	73	-
MMv (kDa)	243	18	177	21

Table 2 EDS analyses of the ash of samples CC and CCD

Chemical element	Sample CC	C	O	Na	Mg	Al	Si	Cl	P	Ca	Cr	Fe	Total
Average content (%)		2.47	48.57	8.00	0.72	0.17	13.65	-	0.83	24.87	0.15	1.07	100
Chemical element	Sample CCD	C	O	Na	Mg	Al	Si	Cl	P	Ca	Cr	Fe	Total
Average content (%)		-	49.35	13.72	0.19	-	16.43	1.08	-	14.59	2.83	1.80	100

shock led to a substantial reduction of particle diameter, reaching the nanometric scale. It should be noted that the DLS technique considers the hydrodynamic diameter of the analyzed particles (without considering the surrounding water molecules) (Ruseva et al. 2018). The results also demonstrated that it was possible to produce nanochitosan from a commercial chitosan that had fairly low purity.

It can be seen from the graph combining the results obtained by DLS (size distributions according to particle number and volume) and viscometry (Fig. 2) that there was good correlation between the molar mass values and the average particle sizes, with small particle size (< 100 nm) being associated with low molar mass (< 25 kDa).

Scanning electron microscopy analyses

The SEM micrographs showed that the depolymerization of the chitosan significantly reduced the size of the particles/agglomerates, making them more uniform, as evidenced by comparing the micrographs for CC and CCD and for SSC and SSCD (Figs. 3 and 4).

The particles/agglomerates of CC sample were considerably larger (sizes up to 600 μm) than those of the SSC (sizes up to 200 μm), showing that the chitosan obtained from the freshwater shrimp shells was much finer than the CC. Similarly, nanochitosan samples presented different particle sizes, with the SSCD consisting of much smaller particles than the CCD, since the precursor material (SSC) also consisted of finer particles, before depolymerization. These results were in

agreement with those obtained by DLS ("Dynamic light scattering"; Figs. 1 and 2).

Therefore, in addition to significantly reducing the size of the chitosan particles/agglomerates, the depolymerization process made them more homogeneous, with regular shapes, while the increased specific surface areas of the materials facilitated their solubilization.

X-ray diffraction analyses

The diffractograms of the chitosan samples (Fig. 4) showed amorphous haloes attributed to semicrystalline structure typical of natural biopolymers. The SSC and CC samples presented well-defined crystalline peaks at 2θ of around 10° and 20°, with the peak at 10° assigned to the reflections of the (010) crystalline planes of the orthorhombic crystals of the α-chitin structure, while the asymmetric peak at 20° was due to the (110) and (020) planes (Alves et al. 2017). However, the crystallinity (determined by the EVA software) of SSC (55.6%) was greater than that of CC (38.1%), as confirmed by the better definition and higher intensity of the SSC crystalline peaks, which could be explained by the different techniques used to produce the materials. The diffractograms obtained for the SSCD and CCD nanochitosans showed that the depolymerization process significantly reduced the crystallinities of the materials, with values of 25.4% for CCD and 25.9% for SSCD. This reduction in crystallinity after formation of the chitosan nanoparticles was mainly due to the destruction of the (010) planes by the thermal shock treatment, with the consequent disappearance of the

Fig 1 Dynamic light scattering measurements of the particle size distributions according to volume (**a**) and number (**b**): commercial chitosan (CC), shrimp shell chitosan (SSC), commercial chitosan after depolymerization (CCD), and shrimp shell chitosan after depolymerization (SSCD)
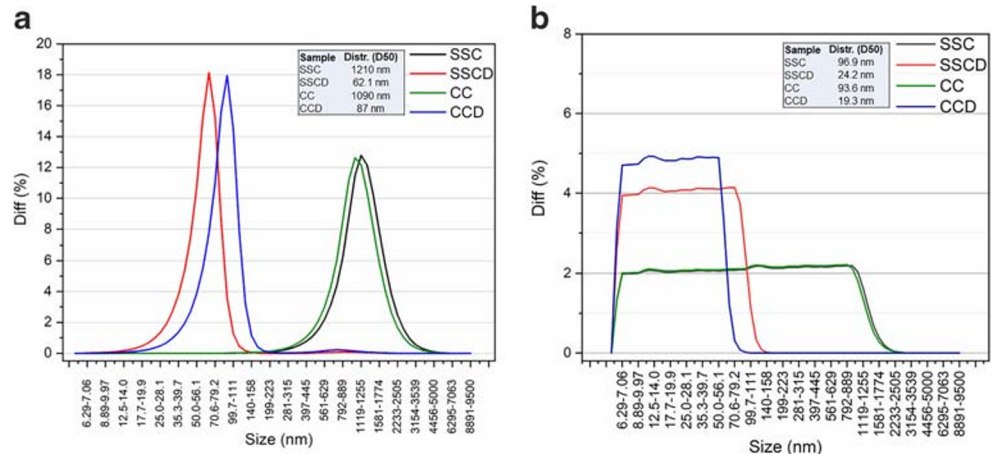
Fig. 2 Dynamic light scattering (particle size distributions by volume and number) and viscometric molar mass results for the commercial and shrimp shell chitosans before (CC and SSC) and after depolymerization (CCD and SSCD). *S1, S2, S3, and S4: other chitosans produced by the same research group; S4D: chitosan S1 after depolymerization
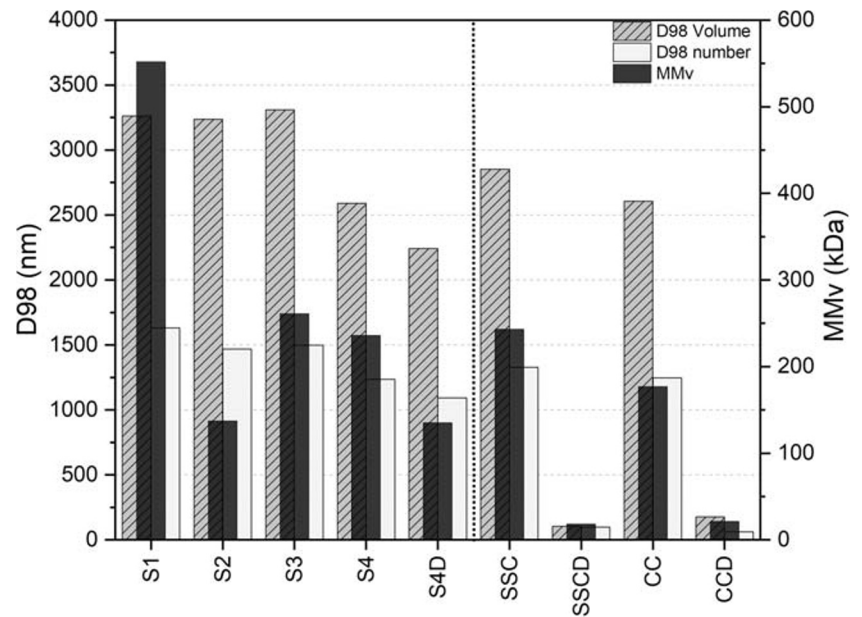

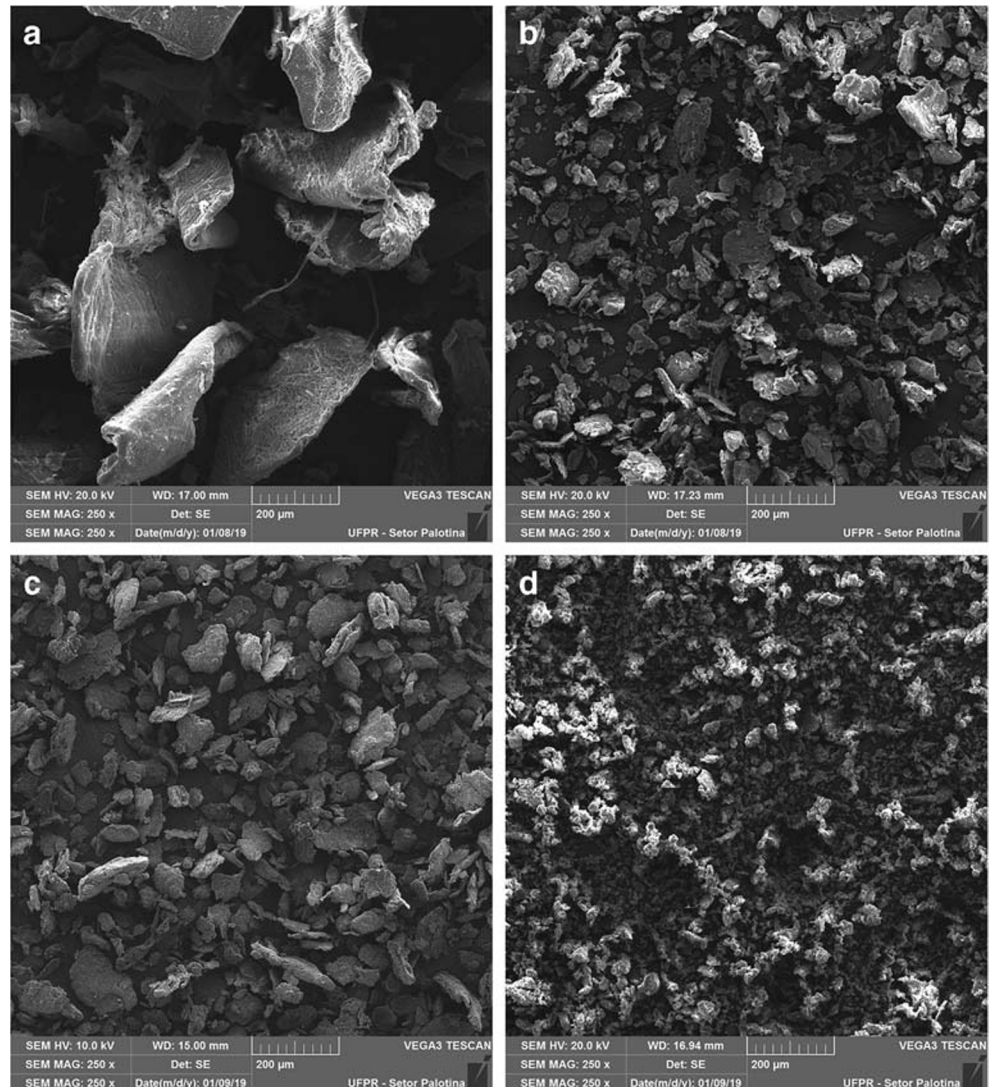**Fig. 3** SEM micrographs of CC before (**a**) and after (**b**) depolymerization, SSC before (**c**) and after (**d**) depolymerization
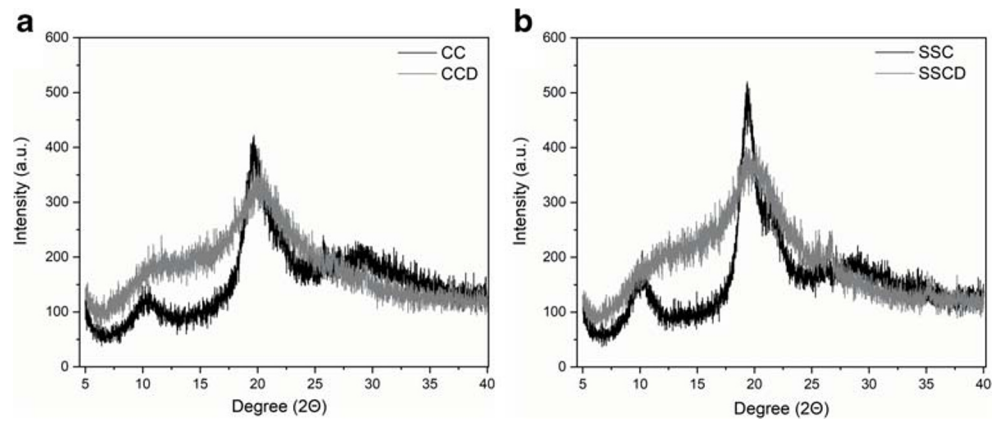
Fig. 4 X-ray diffractograms of the chitosan samples CC and CCD (**a**) and SSC and SSCD (**b**). Crystallinities of the samples: 38.1% (CC), 25.4% (CCD), 55.6% (SSC), and 25.9% (SSCD)


crystalline peak at 10°. The lower crystallinities of the nanochitosans could also be attributed to partial destruction of the (110) and (020) planes during depolymerization, which contributed to broadening of the peak at 20°.

The diffractograms of the SSCD and CCD nanochitosans were generally very similar, so the crystallinity values were close, in agreement with the similar properties of the two samples, especially in terms of DD and MMv (Table 1).

Therefore, the reduction of crystallinity was associated with a decrease in the size of crystalline domains in the semi-crystalline structure of the chitosan, caused by the depolymer-ization process. It is possible that the stresses created during cooling in the thermal shock treatment were attenuated in the final powder grinding stage, which was associated with the breaking of bonds and consequent decreased size of the crys-tallites. It should be noted that since there were increases of the

Fig. 5 HRTEM micrographs of samples CC (**a**, **b**) and SSC (**c**, **d**), acquired under cryogenic conditions
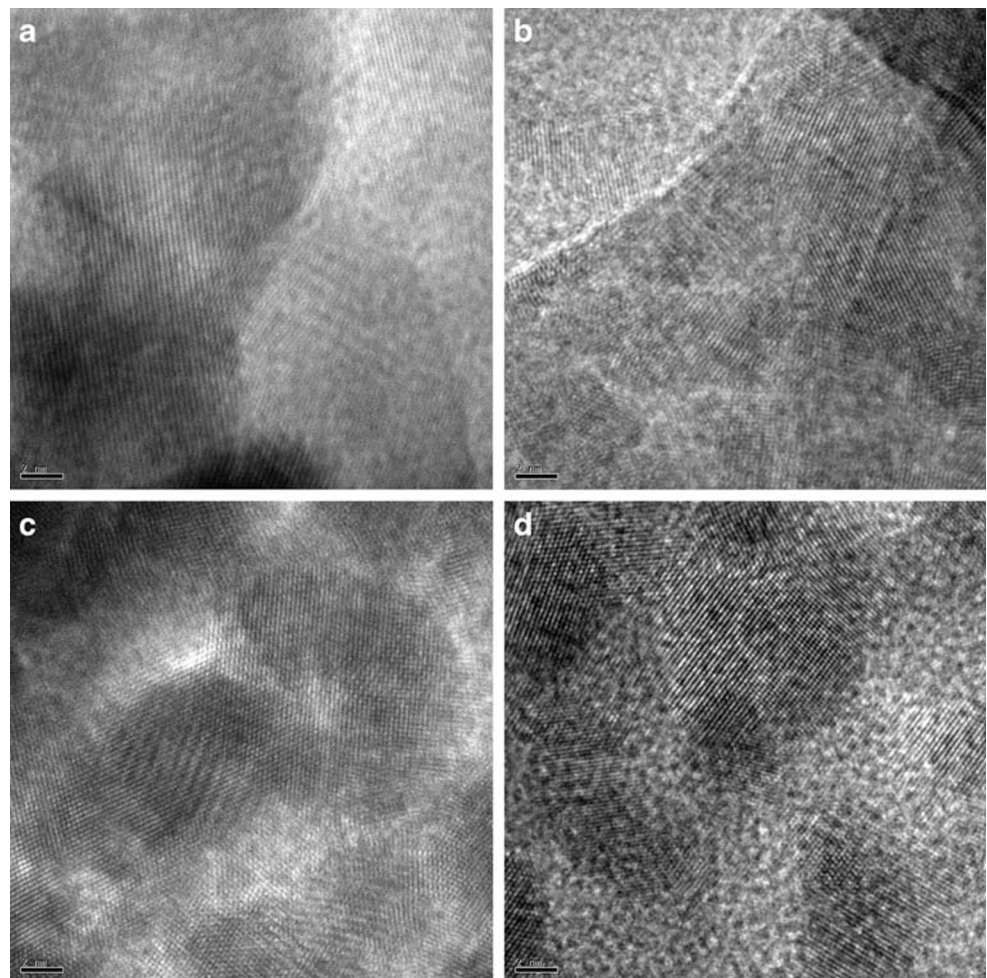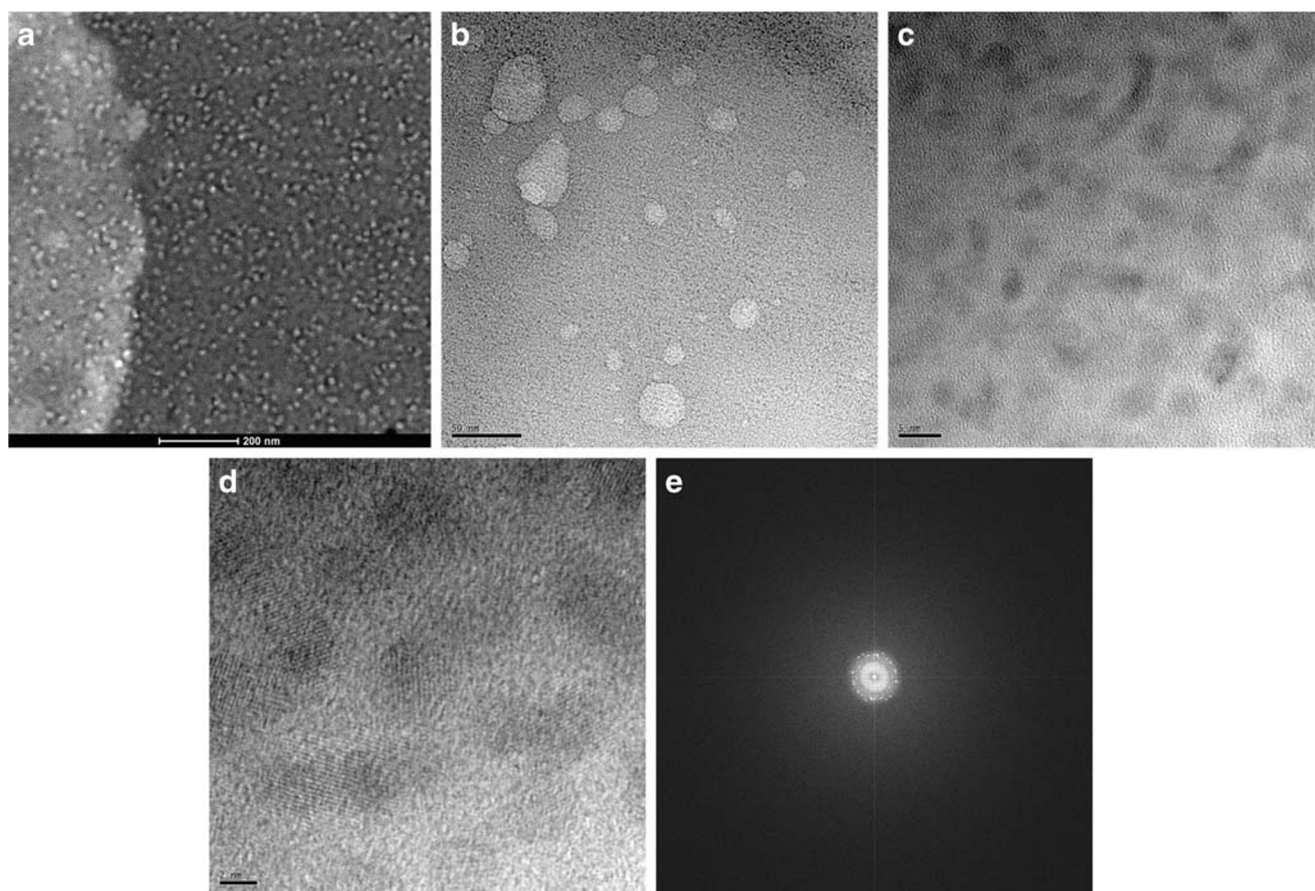
Fig. 6 TEM micrographs of the CCD nanochitosan obtained under cryogenic conditions, at different magnifications: **a** highlighting crystalline regions of the nanoparticles (clear areas revealed by the EVAtool); **b** showing nanoparticles; **c, d** HRTEM images highlighting the crystalline domains; **e** crystalline domains evidenced using selected area electron diffraction (SAED)

amorphous characteristics for the SSCD and CCD samples, there would be a very large error in determination of the crystallite size using the Scherrer equation (Alves et al. 2017). For this reason, transmission electron microscopy (TEM) was employed as an auxiliary technique ("Transmission electron microscopy").

Transmission electron microscopy

The HRTEM micrographs of CC and SSC samples (Fig. 5) clearly revealed crystalline domains with different orientations and sizes, including a predominance of large crystalline regions that even exceeded the areas covered by the images, immersed in an amorphous matrix. These features were typical of semicrystalline materials, such as the chitosans investigated here. The use of TEM analyses performed at cryogenic temperature (employing liquid nitrogen in a holder containing the sample) enabled the acquisition of high quality micrographs of polymeric materials, at high resolution, without risk of decomposition of the sample due to contact with the electron beam of the microscope. Such analyses at cryogenic temperatures have rarely been

reported in the literature concerning the characterization of chitosans.

The micrographs of the CCD and SSCD nanoparticles (Figs. 6a, b and 7a, b, respectively) showed that most of the particles were circular in shape, with diameters between 5 and 90 nm. The micrographs shown in Figs. 6a and 7a were obtained using a TEM tool that selectively highlighted particles with crystalline domains (light areas), which confirmed the presence of many small nanoparticles (< 50 nm) and predominance of crystalline domains in both samples. When the high-resolution (HRTEM) mode was used, the micrographs evidenced various regions of crystalline domains associated with chitosan nanoparticles (Figs. 6c, d and 7c, d). In most of the regions identified, these crystalline domains had circular shapes and diameters ranging from 5 to 10 nm. The acquisition of micrographs using selected area electron diffraction (SAED), shown in Figs. 6e and 7e for samples CCD and SSCD, respectively, confirmed the presence of crystalline domains in the regions highlighted in Figs. 6d and 7d.

The interplanar distance (d_{real}) values were determined from the stacking of planes observed in the crystalline
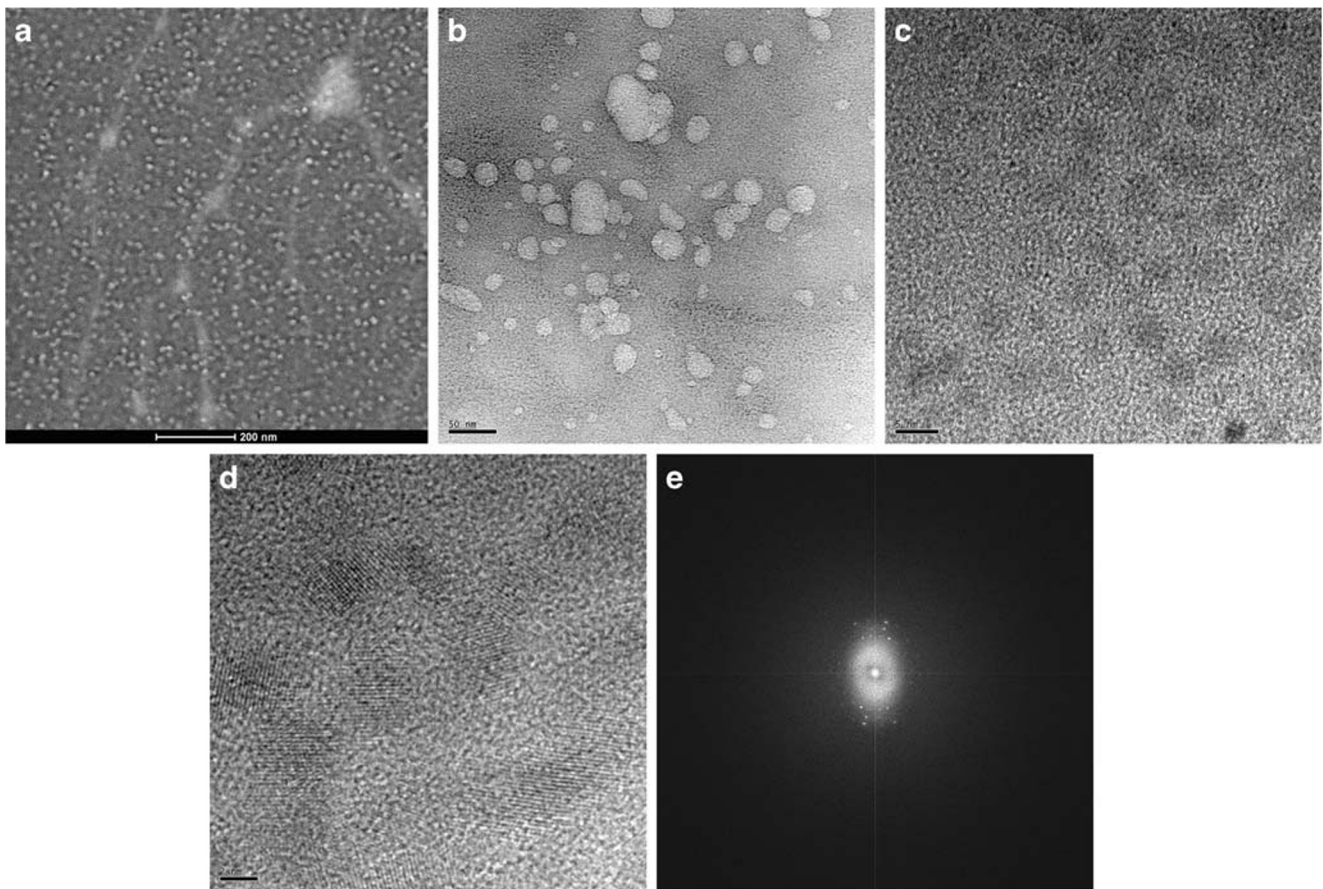
Fig. 7 TEM micrographs of the SSCD nanochitosan obtained under cryogenic conditions, at different magnifications: **a** highlighting crystalline regions of the nanoparticles (clear areas revealed by the EVAtool); **b** showing nanoparticles; **c, d** HRTEM images highlighting the crystalline domains; **e** crystalline domains evidenced using selected area electron diffraction (SAED)

domains of the nanochitosans (Figs. 6d and 7d), with average values of 2.22 and 2.25 Å obtained for the CCD and SSCD nanochitosans, respectively. The d_{real} values were associated with the distances between the (110) planes, corresponding to the most intense crystalline haloes observed in the sample diffractograms (Fig. 8).

TEM analyses showed that the nanoparticles of the CCD and SSCD samples had very similar characteristics, corroborating the features found in the DLS analyses. These results confirmed the efficiency of the methods used to obtain nanochitosan from freshwater shrimp shells, as well as from commercial chitosan.
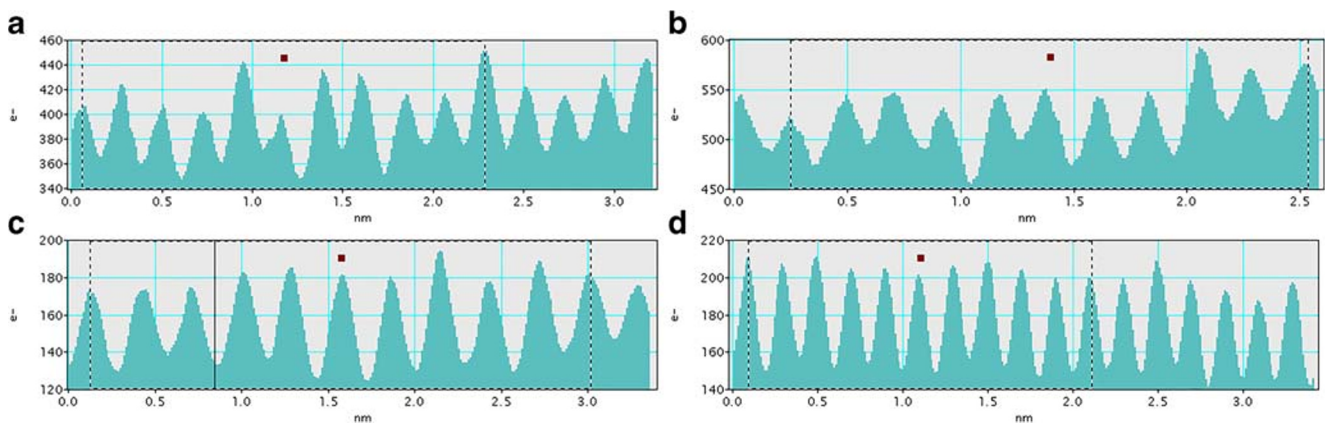

Fig. 8 Representative graphs for stacking of the crystallographic planes in the crystalline domains identified in Figs. 6d and 7d for the CCD (**a, b**) and SSCD (**c, d**) nanochitosans, respectively. The peaks represent the interaction of the electron beam with the atoms of the crystalline planes. The real interplanar distance (d_{real}) was determined as the average of the distances between the peaks

Conclusions

The findings of this work demonstrated that physical grinding procedures, under controlled conditions, followed by thermal shock treatment, were highly effective for production of nanochitosan from a high purity raw material, as well as for depolymerization of a commercial chitosan that was of low quality in terms of homogeneity and the presence of impurities.

DLS analyses revealed that all particles had diameters smaller than 223 nm with an average diameter below 25 nm, finding out reductions in molar mass of up to 13.5-fold after depolymerization. The obtaining of nanochitosan was also confirmed by TEM through the observation of crystalline domains with a diameter between 5 and 10 nm throughout the sample.

Low molar mass nanochitosan was obtained using low-cost methods applied to raw materials that did not need to meet strict quality standards, consequently adding value in biopolymer production chain, which should encourage new studies aimed at expanding the possible applications of these materials.

The results obtained in this research on a pilot scale satisfactorily reproduced those previously found on the bench scale. This demonstrates that the scale increase occurred appropriately generating a significant advance in the maturity of the technology involved in obtaining the nanochitosan, which encourages future research for a further expansion of the production scale.

Authors' contributions Helton José Alves: conceptualization; methodology; writing—review and editing; supervision.

Lázaro José Gasparrini: methodology; formal analysis and investigation.

Felipe Eduardo Bueno Silva: formal analysis and investigation.

Laressa Caciano: formal analysis and investigation.

Graciela Ines Bolzon de Muniz: writing—review and editing.

Eduardo Luis Cupertino Ballester: formal analysis; writing—review and editing.

Paulo André Cremonez: writing—original draft preparation; writing—review and editing.

Mabel Karina Arantes: writing—original draft preparation; writing—review and editing.

Data availability Data sharing is not applicable to this article as no datasets were generated or analyzed during the current study.

Compliance with ethical standards

Competing interests The authors declare that they have no competing interests.

Ethical approval and consent to participate The manuscript does not report on or involve the use of any animal or human data.

Consent for publication Not applicable.

References

Alves HJ, Furman M, Kugelmeier CL, De Oliveira CR, Bach VR, Lupatini KN, Neves AC, Arantes MK (2017) Effect of shrimp shells milling on the molar mass of chitosan. Polímeros 27:41–47

Alves HJ, Vieceli M, Alves C, Muñiz GIB, De Oliveira CLP, Feroldi M, Arantes MK (2018) Chitosan depolymerization and nanochitosan production using a single physical procedure. J Polym Environ 26:3913–3923

Arantes MK, Kugelmeier CL, Cardozo-Filho L, Monteiro MR, Oliveira CR, Alves HJ (2014) Influence of the drying route on the depolymerization and properties of chitosan. Polym Eng Sci 55:1969–1976

Bakshi PS, Selvakumar D, Kadirvelu K, Kumar NS (2018) Comparative study on antimicrobial activity and biocompatibility of N-selective chitosan derivatives. React Funct Polym 124:149–155

Carvalho FG, Magalhães TC, Teixeira NM, Gondin BLV, Carlo HL, Santos RL, Oliveira AR, Denadai AML (2019) Synthesis and characterization of TPP/chitosan nanoparticles: colloidal mechanism of reaction and antifungal effect on C. albicans biofilm formation. Mater Sci Eng C 104:109885

Egladir MA, Uddin S, Ferdosh S, Adam A, Chowdhury AJK, Sarker Z (2015) Impact of chitosan composites and chitosan nanoparticle composites on various drug delivery systems: a review. J Food Drug Anal 23:619–629

Fan W, Yan W, Xu Z, Ni H (2012) Formation mechanism of monodisperse, low molecular weight chitosan nanoparticles by ionic gelation technique. Colloid Surface B 90:21–27

Gonil P, Sajomsang W (2012) Applications of magnetic resonance spectroscopy to chitin from insect cuticles. Int J Biol Macromol 51:514–522

Gupta VK, Fakhri A, Agarwal S, Azad M (2017) Synthesis and characterization of Ag2S decorated chitosan nanocomposites and chitosan nanofibers for removal of lincosamides antibiotic. Int J Biol Macromol 103:1–7

Kasaai MR (2007) Calculation of Mark–Houwink–Sakurada (MHS) equation viscometric constants for chitosan in any solvent–temperature system using experimental reported viscometric constants data. Carbohydr Polym 68:477–4885

Mitall H, Ray SS, Kaith BS, Bhatia JK, Sharma J, Alhassan SM (2018) Recent progress in the structural modification of chitosan for applications in diversified biomedical fields. Eur Polym J 109:402–434

Muanprasat C, Chatsudthipong V (2017) Chitosan oligosaccharide: biological activities and potential therapeutic applications. Pharmacol Therapeut 170:80–97

Nagpal K, Singh SK, Mishra DN (2013) Optimization of brain targeted chitosan nanoparticles of Rivastigmine for improved efficacy and safety. Int J Biol Macromol 59:72–83

Neves A, Zanette C, Grade ST, Schaffer JV, Alves HJ, Arantes MK (2017) Optimization of lactic fermentation for extraction of chitin from freshwater shrimp waste. Acta Sci-Technol 39:125–133

Panit N, Wichaphon J, Lertisiri S, Niamsiri N (2016) Effect of physical and physicochemical characteristics of chitosan on fat-binding capacities under in vitro gastrointestinal conditions. LWT-Food Sci Technol 71:25–32

Pant A, Negi JS (2018) Novel controlled ionic gelation strategy for chitosan nanoparticles preparation using TPP-β-CD inclusion complex. Eur J Pharm Sci 112:180–185

Perez JJ, Francois NJ (2016) Chitosan-starch beads prepared by ionotropic gelation as potential matrices for controlled release of fertilizers. Carbohydr Polym 148:134–142

Perez JJ, Francois NJ, Maroniche GA, Borrajo MP, Pereyra MA, Creus CM (2018) A novel, green, low-cost chitosan-starch hydrogel as potential delivery system for plant growth-promoting bacteria. Carbohydr Polym 202:409–417

Rao MS, Stevens WF (2006) Fermentation of shrimp biowaste for chitin production. Food Bioprocess Technol 44:83–87

Rinaudo M (2006) Chitin and chitosan: properties and applications. Prog Polym Sci 31:603–632

Ruseva V, Lyons M, Powell J, Austin J, Malm A, Corbett J (2018) Capillary dynamic light scattering: continuous hydrodynamic particle size from the nano to the micro-scale. Colloid Surface A 558: 504–511

Santos ZM, Caroni ALPF, Pereira MR, Da Silva DR, Fonseca JLC (2009) Determination of deacetylation degree of chitosan: a comparison between conductometric titration and CHN elemental analysis. Carbohydr Res 344:2591–2595

Soares PIP, Sousa AI, Silva JC, Ferreira IMM, Novo CMM, Borges JP (2016) Chitosan-based nanoparticles as drug delivery systems for doxorubicin: optimization and modelling. Carbohydr Polym 147: 304–312

Tang Z, Qian J, Shi L (2007) Preparation of chitosan nanoparticles as carrier for immobilized enzyme. Appl Biochem 136:77–96

Tsai G-J, Su W-H, Chen H-C, Pan C-L (2002) Antimicrobial activity of shrimp chitin and chitosan from different treatments and applications of fish preservation. Fish Res 68:170–177

Van Der Gronde T, Hartog A, Van Hess C, Pellikaan H, Pieters T (2016) Systematic review of the mechanisms and evidence behind the hypocholesterolaemic effects of HPMC, pectin and chitosan in animal trials. Food Chem 199:746–759

Wang X, Du Y, Fan L, Liu H, Hu Y (2005) Chitosan- metal complexes as antimicrobial agent: synthesis, characterization and Structure-activity study. Polym Bull 55:105–113

Wang J-P, Chen Y-Z, Yuan S-J, Sheng F-P, Yu H-Q (2009) Synthesis and characterization of a novel cationic chitosan-based flocculant with a high water-solubility for pulp mill wastewater treatment. Water Res 43:5267–5275

Wu L, Liu M (2008) Preparation and properties of chitosan-coated NPK compound fertilizer with controlled-release and water-retention. Carbohydr Polym 72:240–247

Ye B, Zheng R, Ruan X, Zheng Z, Cai H (2018) Chitosan-coated doxorubicin nano-particles drug delivery system inhibits cell growth of liver cancer via p53/PRC1 pathway. Biochem Bioph Res Co 495: 414–420

Zimmermann AC, Mecabô A, Fagundes T, Rodrigues CA (2010) Adsorption of Cr (VI) using Fe-crosslinked chitosan complex (Ch-Fe). J Hazard Mater 179:192–196